Journal of Materials Chemistry A

ROYAL SOCIETY OF CHEMISTRY

PAPER

View Article Online
View Journal | View Issue



Cite this: J. Mater. Chem. A, 2023, 11, 9824

# Overall water electrolysis on a graphdiyne-iron oxyhydroxide heterostructure†

Xi Chen,[ac] Danyan Zhang,[ac] Xuchen Zheng,[ac] Chao Zhang,[ac] Yang Gao,[a] Chengyu Xing,[a] Siao Chen,[ac] Han Wu,[ac] Yurui Xue *[ab] and Yuliang Li *[ac]

Received 24th February 2023
Accepted 12th April 2023

DOI: 10.1039/d3ta01176c

rsc.li/materials-a

Water electrolysis provides an effective method for energy efficient hydrogen production. The challenge in this field is how to synthesize electrocatalysts with high activity and stability in water electrolysis reactions. Herein, a new heterostructure of graphdiyne-iron oxyhydroxide was synthesized by controlled growth of GDY films on the surface of FeOOH nanowires (FeOOH@GDY). An interface structure with an electron-donor (GDY) and electron-acceptor (Fe) was formed, which showed the obvious incomplete charge transfer between GDY and Fe atoms at the interfaces. This produces infinite active sites which guarantee excellent catalytic activity. The GDY grown on the surfaces of oxyhydroxides endows the electrocatalyst with high stability. These unique and fascinating properties make FeOOH@GDY show excellent catalytic activities toward overall water splitting (OWS) with a small cell voltage of 1.43 V at 10 mA $cm^{-2}$ under ambient conditions and excellent long-term stability.



## Introduction

Hydrogen ($H_2$), a clean-energy carrier/fuel with the potential to replace hydrocarbons, plays an important role in a future sustainable energy system.[1] Water electrolysis which contains the hydrogen evolution reaction (HER) and the oxygen evolution reaction (OER) has been widely considered to be an ideal method for efficient $H_2$ production and has attracted largely increased attention from researchers over the past few decades.[2–4] However, the sluggish reaction kinetics for the HER and OER seriously limits the overall performance of a water electrolysis device. To overcome this application performance bottleneck, extensive efforts have been made to develop electrocatalysts with high activity and stability. Unfortunately, electrocatalysts with high electrocatalytic performances were usually noble-metal-based materials such as Pt/C for the HER and $RuO_2$/$IrO_2$ for the OER.[5–7] Their high cost, scarcity, and poor stability in strong acid or alkali media are limitations to their practical applications. The rational design and synthesis of active, stable and low-cost electrocatalysts are still of great importance.

Among various methods for enhancing catalytic performances, constructing efficient interface structures by incorporating catalysts with carbon materials can effectively improve the electrocatalytic selectivity, activity, and stability by enhancing the conductivity, stability, and the number of surface-active sites and the adsorption/desorption ability of reactants/intermediates.[8–10] However, traditional carbon-based materials are usually prepared under extremely harsh conditions, which could easily destroy the composition and structure of active sites and result in low catalytic activity and stability.

Compared with traditional carbon-based materials, GDY shows many fascinating characteristics for electrocatalysis, including sp-/$sp^2$-cohybridized and large π-conjugated all-carbon two-dimensional networks, natural pores, large specific surface area, high conductivity, high intrinsic activity, and excellent stabilities.[11–14] Specifically, the uneven charge distribution on the surface of GDY endows it with infinite active sites and high intrinsic activity. And the unique property of GDY that it can be controllably grown on arbitrary material surfaces allows the selective construction of active interfaces with determined composition and structures. Moreover, the unique incomplete charge transfer between GDY and metal atoms could increase the number and the stability of the active site.[15–18] Benefitting from these superiorities, GDY has shown excellent performances and attracted greatly increasing interest from the fields of electrocatalysis,[19–28] photocatalysis,[29–31] energy conversion,[32–37] *etc.*[38–40]

In this study, the highly active and stable OER, HER, as well as OWS were achieved on the heterostructure of FeOOH@GDY with electronic-donating and withdrawing interface structures, resulting in infinite active sites which guarantee excellent

[a]CAS Key Laboratory of Organic Solids, Institute of Chemistry, Chinese Academy of Sciences, Beijing 100190, China. E-mail: ylli@iccas.ac.cn

[b]Shandong Provincial Key Laboratory for Science of Material Creation and Energy Conversion, Science Center for Material Creation and Energy Conversion, School of Chemistry and Chemical Engineering, Shandong University, Jinan 250100, China. E-mail: yrxue@sdu.edu.cn

[c]University of Chinese Academy of Sciences, Beijing 100049, China

† Electronic supplementary information (ESI) available. See DOI: https://doi.org/10.1039/d3ta01176c

catalytic activity. The GDY grown on surfaces of oxyhydroxides endows the electrocatalyst with high stability. For example, FeOOH@GDY shows small overpotentials of 205 and 38 mV at 10 mA $cm^{-2}$ for the OER and HER in 1.0 M KOH. When assembled into an electrolyzer, the catalyst can drive 10 mA $cm^{-2}$ at a low cell voltage of 1.43 V for more than 115 hours.

## Results and discussion

### Synthesis and structural characterization

The electrocatalysts of FeOOH@GDY heterostructures were synthesized through a simple two-step method (Fig. 1). In brief, a three-dimensional (3D) electrode was prepared by the growth of a film of FeOOH nanowires on the surface of 3D carbon networks (FeOOH NWs). SEM images (Fig. 2a–c) show that the FeOOH NWs were uniformly and densely grown on the smooth surface of CC (Fig. S1†). The obtained FeOOH NWs were then used as substrates for the *in situ* growth of GDY *via* a typical coupling reaction. After the completion of the reaction, FeOOH@GDY heterostructured catalysts were obtained. As shown in Fig. 2d–f, the nanowire morphology was well maintained, but the surface of the nanowires became rougher after the *in situ* growth of GDY. The photograph displays the successful preparation of a centimeter-scale FeOOH@GDY electrode with a uniform surface (Fig. 2g). The FeOOH@GDY electrodes could be bent more than 180° without breaking (Fig. 2h), indicating their high flexibility which is beneficial for the assembly of electrolysis devices. Contact measurement (Fig. 2i) demonstrates the superhydrophilic properties of FeOOH@GDY which are beneficial for facilitating mass/ion diffusion at the electrolyte–catalyst interface and improving the performance of a catalyst.[19,25]

TEM images confirm the nanowire morphology of FeOOH NWs with an average diameter of ~30 nm (Fig. 3a) and a polycrystalline structure (Fig. 3b–d). As characterized by HRTEM (Fig. 3c and d), FeOOH NWs have two types of lattice spacings of 0.269 and 0.245 nm, which can be ascribed to the (130) and (111) planes of FeOOH, respectively. After *in situ* growth of GDY on FeOOH, the nanowire width increases to ~40 nm (Fig. 3e). The intimate interface between the FeOOH and GDY (Fig. 3f) confirms

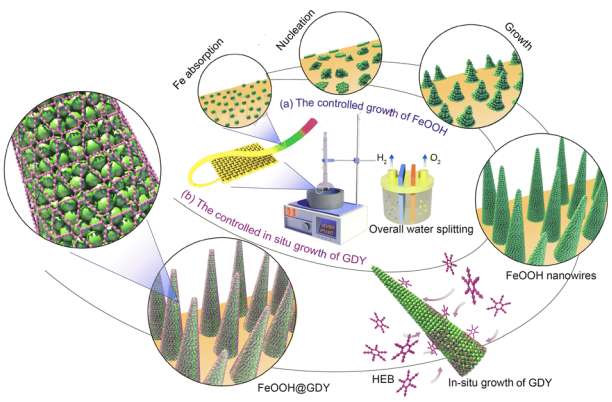


Fig. 1 Schematic representation of the controlled synthesis route to FeOOH@GDY through (a) the growth of FeOOH nanowires and (b) the *in situ* growth of GDY.

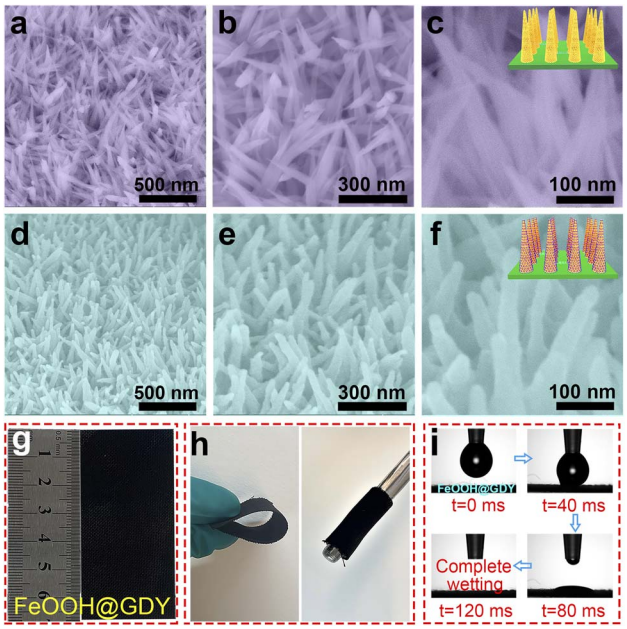


Fig. 2 The SEM images of (a–c) FeOOH nanowire electrode and (d–f) FeOOH@GDY electrode. (g) The optical images of the FeOOH@GDY electrode and (h) its various bending configurations. (i) The contact angle measurement of FeOOH@GDY.

the successful construction of the heterostructure of FeOOH@GDY. Fringe spacing of GDY increased from 0.365 nm (pure GDY, Fig. S2†) to 0.385 nm (FeOOH@GDY, Fig. 3g), and the lattice distance of the (130) plane of FeOOH decreased to 0.256 nm. Interestingly, after the growth of GDY on the surface of FeOOH, the crystal phase of (111) disappeared. Elemental mapping images (Fig. 3i) show homogeneous distribution of Fe, O, and C elements over the FeOOH@GDY nanowire. The change in the crystal structure of FeOOH was further confirmed by the XRD results. As shown in Fig. 3j, FeOOH shows two obvious peaks

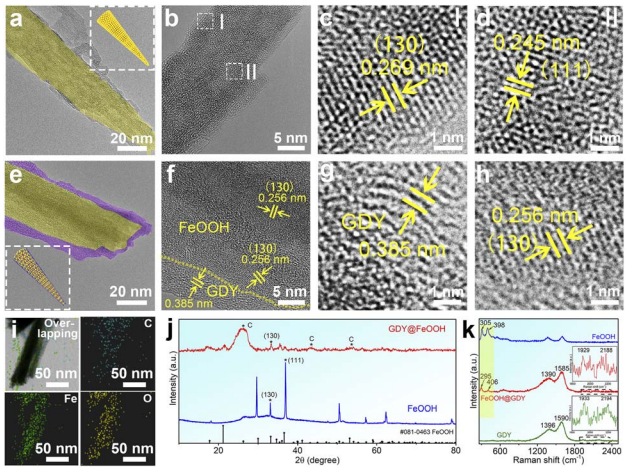


Fig. 3 The low- and high-resolution TEM images of (a–d) FeOOH NWs and (e–h) FeOOH@GDY. (i) The overlapping images and elemental mapping images of C, Fe, and O in FeOOH@GDY. (j) The XRD patterns of FeOOH and FeOOH@GDY powders scraped from electrodes. (k) The Raman spectra of FeOOH, GDY, and FeOOH@GDY.

at 34.7° and 36.6° which correspond to (130) and (111), respectively (ICDD PDF # 081-0436). Only the (130) phase could be observed in FeOOH@GDY. These results reveal that the *in situ* growth of GDY effectively induces the transition of the (111) phase to the catalytically active (130) phase,[41,42] which helps improve the catalytic activity. Raman spectra (Fig. 3k) show that FeOOH@GDY contains two dominant regions of FeOOH species (295 and 406 $cm^{-1}$) and GDY (D band: 1396 $cm^{-1}$; G band: 1590 $cm^{-1}$; diyne links: 1933 and 2194 $cm^{-1}$), further confirming the successful incorporation of FeOOH and GDY. This was also confirmed by the infrared spectrometry (IR; Fig. S3†). Compared with pure GDY and FeOOH, the peaks exhibit negative shifts, which indicates the strong interactions between FeOOH and GDY.[25] In addition, FeOOH@GDY has a larger intensity ratio of D and G bands ($I_D/I_G$) of 0.97 than pure GDY (0.89), indicating the formation of more defects after the growth of GDY, which helps improve the electrochemical activity.[15]

The chemical states of the samples were further studied by X-ray photoelectron spectroscopy (XPS). After the *in situ* growth of GDY on FeOOH, the intensity of the C 1s peak is greatly enhanced. Fig. 4a shows the C 1s XPS spectrum of GDY with four characteristic peaks corresponding to C–C ($sp^2$), C–C (sp), C–O, and C=O, and a C–C ($sp^2$) to C–C (sp) ratio of 0.5. For FeOOH@GDY, two additional peaks at 283.2 and 289.55 eV corresponding to C–Fe and π–π* transitions, respectively, were observed. The formation of a C–Fe bond would effectively enhance the stability of the formed interface structures. Besides, the XPS survey spectra (Fig. S4†) show the co-existence of C, O, and Fe in FeOOH@GDY. These further confirm the successful growth of GDY on FeOOH NWs. The high-resolution Fe 2p XPS spectra of FeOOH and FeOOH@GDY shown in Fig. 4b are well fitted into two spin–orbit doublets of $Fe^{2+}$ (at 710.35 and 723.87 eV) and $Fe^{3+}$ (at 712.37 and 726.70 eV).[43] Compared with those of GDY, C 1s XPS peaks of FeOOH@GDY shift to higher binding energies (BEs) by 0.21 eV and the Fe 2p XPS peaks of FeOOH@GDY shift to lower BEs, which indicates the efficient charge transfer from GDY to FeOOH. The O 1s XPS spectra (Fig. 4c) could be divided into O–Fe (529.68 eV), –OH (531.35 eV), and $H_2O$ (531.5 eV) species, respectively. The valence spectra (Fig. 4d) show that the top of the valence band of FeOOH@GDY ($\Delta E$ = 1.33 eV) is closer to the Fermi level than those of GDY ($\Delta E$ = 1.54 eV) and FeOOH ($\Delta E$ = 1.67 eV), indicating the improved conductivity of the catalyst. In order to examine the components of FeOOH@GDY from the surface to the inner part, XPS depth profiling (C 1s, Fe 2p and O 1s) was conducted (Fig. 4e).[25] As the etching depth increases, the C 1 s (Fig. 4f), Fe 2p (Fig. 4g) and O 1s (Fig. 4h) XPS spectra of FeOOH@GDY show that there are no changes in the compositions and chemical states of FeOOH@GDY, indicating the robust stability of the catalyst. As the etching depth increases, the content of Fe increases while the content of C decreases (Fig. 4i), confirming the successful coating of GDY on FeOOH.

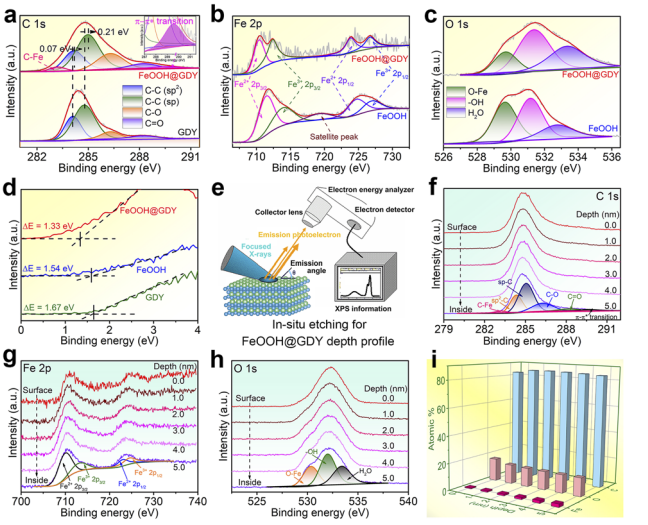


Fig. 4 (a) The high-resolution C 1s XPS spectra of GDY and FeOOH@GDY. The high-resolution (b) Fe 2p and (c) O 1s XPS spectra of FeOOH and FeOOH@GDY. (d) The valence spectra of FeOOH@GDY, FeOOH, and GDY (e) Schematic representation of the depth profiling experiments. The sets of (f) C 1s, (g) Fe 2p, and (h) O 1s XPS spectra of FeOOH@GDY measured during the depth profiling experiments. (i) The atomic percentages of C, Fe, and O in FeOOH@GDY obtained from the depth profiling experiments.

## Electrocatalytic performance studies

The OER catalytic activity of FeOOH@GDY was first tested in 1.0 M KOH. Samples with different GDY contents have been synthesized and tested. The FeOOH@GDY sample with a GDY content of 1.5 mg $cm^{-2}$ has the best catalytic activity (Fig. S5†). Fig. 5a shows that FeOOH@GDY has the best OER activity with the lowest overpotential of 205 mV at 10 mA $cm^{-2}$ compared to GDY (384 mV), FeOOH (444 mV), $RuO_2$ (394 mV) and CC (862

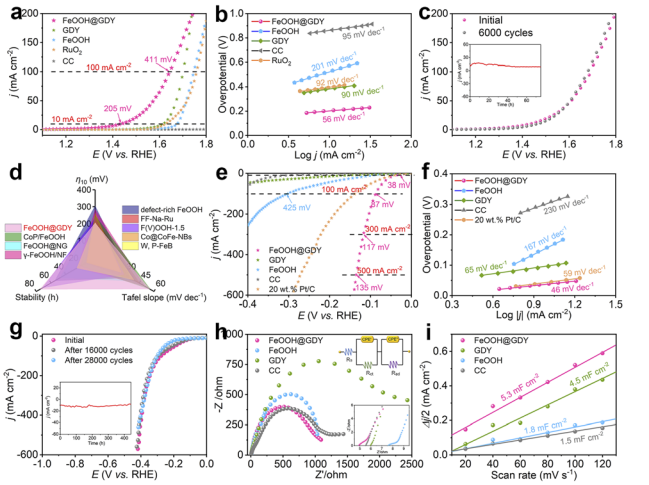


Fig. 5 OER and HER performances of the catalysts in 1.0 M KOH solution. (a) OER polarization curves and (b) corresponding Tafel plots of the samples. (c) Polarization curves of FeOOH@GDY before and after OER CV cycling tests (inset: the time-dependent current density curve). (d) Comparison of the OER catalytic activity of FeOOH@GDY with the reported FeOOH-based catalysts. (e) HER polarization curves and (f) corresponding Tafel plots of the samples. (g) Polarization curves of FeOOH@GDY before and after HER CV cycling tests (inset: the time-dependent current density curve). (h) Nyquist plots of FeOOH@GDY, GDY, FeOOH and CC. The inset displays the magnified plot. (i) Current density differences of different samples against scan rates.

mV). Besides, FeOOH@GDY has a smaller Tafel slope of 56 mV $dec^{-1}$ than GDY (90 mV $dec^{-1}$), FeOOH (201 mV $dec^{-1}$), $RuO_2$ (92 mV $dec^{-1}$), and CC (95 mV $dec^{-1}$), which indicates its superior OER kinetics (Fig. 5b). In addition to excellent OER activity, FeOOH@GDY also shows outstanding stability. As shown in Fig. 5c, there are negligible decreases in current densities after the continuous cycling test for 6000 cycles and long-term chronoamperometry test for over 75 h, while FeOOH NWs show a significant decrease in activity (Fig. S6a†). Such excellent OER performance of FeOOH@GDY is compared favorably to those of many recently reported FeOOH-based electrocatalysts (Fig. 5d and Table S1†).

The HER catalytic performance was further studied in 1.0 M KOH. FeOOH@GDY has the smallest overpotential of 38 mV at 10 mA $cm^{-2}$, better than FeOOH (90 mV@10 mA $cm^{-2}$), GDY (158 mV@10 mA $cm^{-2}$), CC (304 mV@10 mA $cm^{-2}$), 20 wt% Pt/C (43 mV@10 mA $cm^{-2}$) and some reported FeOOH-based electrocatalysts (Fig. 5e and Table S2†). Moreover, FeOOH@GDY shows good HER performance with low overpotentials of 87, 117, 135, and 161 mV at high current density (100, 300, 500 and 1000 mA $cm^{-2}$). The smallest Tafel slope of 46 mV $dec^{-1}$ is shown for FeOOH@GDY in contrast with FeOOH (167 mV $dec^{-1}$), GDY (65 mV $dec^{-1}$), CC (230 mV $dec^{-1}$), and Pt/C (59 mV $dec^{-1}$) in Fig. 5f, revealing the faster reaction kinetics of FeOOH@GDY. The HER on FeOOH@GDY proceeds most likely *via* a Volmer–Heyrovsky mechanism.[44] The applied overpotential shows no significant increases at 10 mA $cm^{-2}$ after 28 000 continuous CV cycling cycles and decrease in the current densities after 441 h electrolysis (Fig. 5g), which demonstrate the excellent long-term stability of FeOOH@GDY. In contrast, FeOOH presented poor stability during the electrolysis process and its HER activity decreased sharply (Fig. S6b†). These results indicate that the heterostructures of GDY and FeOOH could significantly improve the stability of the catalyst.

Nyquist plots were obtained by EIS measurements (Fig. 5h) and fitted with an R(QR)(QR) equivalent circuit model (Fig. S7†) containing the solution resistance ($R_s$), the charge transfer resistance ($R_{ct}$) and the gas adsorption resistance ($R_{ad}$). As presented in Table S3 and Fig. S8,† FeOOH@GDY shows the smallest $R_s$ (4.93 Ω) and $R_{ct}$ (0.31 Ω) compared to FeOOH ($R_s$ = 7.68 Ω, $R_{ct}$ = 1170 Ω), GDY ($R_s$ = 5.98 Ω, $R_{ct}$ = 37.56 Ω) and CC ($R_s$ = 5.49 Ω, $R_{ct}$ = 1080 Ω), indicating the enhanced charge transfer ability and good electrical conductivity of FeOOH@GDY, which could effectively accelerate the catalytic kinetics of the heterostructure. Higher calculated double-layer capacitance ($C_{dl}$) of FeOOH@GDY (5.3 mF $cm^{-2}$) than GDY (4.5 mF $cm^{-2}$), FeOOH (1.8 mF $cm^{-2}$) and CC (1.5 mF $cm^{-2}$) indicates its higher density of catalytically active sites (Fig. 5i and S9†). Accordingly, the calculated electrochemical active surface area (ECSA) of FeOOH@GDY is 132.5 $cm^2$, larger than that of GDY (112.5 $cm^2$), FeOOH (45.0 $cm^2$) and CC (37.5 $cm^2$),[45] demonstrating the largest exposed catalytic sites of FeOOH@GDY to the reactants and higher surface roughness assigned to the introduction of GDY, which is beneficial for the electrolysis. Remarkably, FeOOH@GDY has better catalytic activities for both the OER and HER processes, higher conductivity and larger ECSA than pure FeOOH and GDY. These results indicate that catalytic activity comes from the newly formed interface structures with unique incomplete charge transfer between GDY and Fe atoms.

The water electrolysis measurements were performed in 1.0 M KOH, in which FeOOH@GDY was used as both the cathode and anode (Fig. 6a). FeOOH@GDY||FeOOH@GDY shows the best OWS activity with the lowest cell voltage of 1.43 V (an overpotential of 198 mV) at 10 mA $cm^{-2}$ (Fig. 6b), lower than that of 20 wt% Pt/C||$RuO_2$ (1.63 V), FeOOH||FeOOH (1.64 V), GDY||GDY (1.83 V) and CC||CC (1.85 V). After a 115 h chronopotentiometry test (Fig. 6c), there is negligible variation in both catalytic activity and morphology (Fig. S10†) of FeOOH@GDY, indicating the reliable long-term performance of the FeOOH@GDY||FeOOH@GDY electrode. These results demonstrate the excellent activity and long-term stability of FeOOH@GDY for water electrolysis under alkaline conditions, outperforming other reported Fe-based catalysts (Fig. 6d and Table S4†).

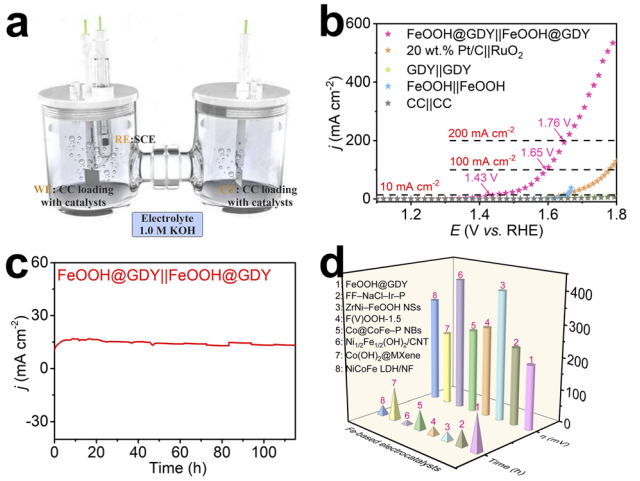


Fig. 6 (a) The schematics of a practical water electrolyzer under working conditions. (b) LSV curves of the catalysts for OWS. (c) The time-dependent current density curve of FeOOH@GDY||FeOOH@GDY. (d) Comparison of the OWS catalytic activity of FeOOH@GDY with that of the reported FeOOH-based catalysts.

## Conclusions

In summary, by perfectly utilizing the advantage that GDY can grow on any substrate, we achieved the *in situ* controlled growth of an interface structure with an electron-donor and electron-acceptor. Detailed structural characterization studies demonstrate that the precise structure of the catalyst, the highly uneven charge distribution on the surface of GDY and charge transfer salt formed greatly improve catalytic performances for the OER, the HER, and OWS. The overpotentials of the HER and OER of FeOOH@GDY are only 38 and 205 mV at 10 mA $cm^{-2}$ in 1.0 M KOH. FeOOH@GDY||FeOOH@GDY can deliver 10 mA $cm^{-2}$ for more than 115 h at a cell voltage of 1.43 V.

## Conflicts of interest

There are no conflicts to declare.

## Acknowledgements

We acknowledge the support from the National Key Research and Development Project of China (2018YFA0703501), the National Natural Science Foundation of China (22021002), and the Key Program of the Chinese Academy of Sciences (XDPB13).

## References

1 A. J. Shih and S. M. Haile, *Science*, 2022, **376**, 348–349.
2 X. Li, L. Zhao, J. Yu, X. Liu, X. Zhang, H. Liu and W. Zhou, *Nano-Micro Lett.*, 2020, **12**, 131.
3 X. Zhang, M. Zhang, Y. Deng, M. Xu, L. Artiglia, W. Wen, R. Gao, B. Chen, S. Yao, X. Zhang, M. Peng, J. Yan, A. Li, Z. Jiang, X. Gao, S. Cao, C. Yang, A. J. Kropf, J. Shi, J. Xie, M. Bi, J. A. van Bokhoven, Y. W. Li, X. Wen, M. Flytzani-Stephanopoulos, C. Shi, W. Zhou and D. Ma, *Nature*, 2021, **589**, 396–401.
4 H. Xie, Z. Zhao, T. Liu, Y. Wu, C. Lan, W. Jiang, L. Zhu, Y. Wang, D. Yang and Z. Shao, *Nature*, 2022, **612**, 673–678.
5 J. Li, W. Xu, J. Luo, D. Zhou, D. Zhang, L. Wei, P. Xu and D. Yuan, *Nano-Micro Lett.*, 2018, **10**, 6.
6 S. Deng, K. Zhang, D. Xie, Y. Zhang, Y. Zhang, Y. Wang, J. Wu, X. Wang, H. J. Fan, X. Xia and J. Tu, *Nano-Micro Lett.*, 2019, **11**, 12.
7 G. Qian, J. Chen, T. Yu, L. Luo and S. Yin, *Nano-Micro Lett.*, 2021, **13**, 77.
8 Y. Fang, Y. Lv, F. Gong, A. A. Elzatahry, G. Zheng and D. Zhao, *Adv. Mater.*, 2016, **28**, 9385–9390.
9 B. Lv, Y. Liu, W. Wu, Y. Xie, J. L. Zhu, Y. Cao, W. Ma, N. Yang, W. Chu, Y. Jia, J. Wei and J. L. Sun, *Nat. Commun.*, 2022, **13**, 1835.
10 X. Lin, H. Su, S. He, Y. Song, Y. Wang, Z. Qin, Y. Wu, X. Yang, Q. Han, J. Fang, Y. Zhang, H. Segawa, M. Grätzel and L. Han, *Nat. Energy*, 2022, **7**, 520–527.
11 G. Li, Y. Li, H. Liu, Y. Guo, Y. Li and D. Zhu, *Chem. Commun.*, 2020, **46**, 3256–3258.
12 C. Huang, Y. Li, N. Wang, Y. Xue, Z. Zuo, H. Liu and Y. Li, *Chem. Rev.*, 2018, **118**, 7744–7803.
13 H. Yu, Y. Xue and Y. Li, *Adv. Mater.*, 2019, **31**, e1803101.
14 Y. Fang, Y. Liu, L. Qi, Y. Xue and Y. Li, *Chem. Soc. Rev.*, 2022, **51**, 2681–2709.
15 Y. Fang, Y. Xue, Y. Li, H. Yu, L. Hui, Y. Liu, C. Xing, C. Zhang, D. Zhang, Z. Wang, X. Chen, Y. Gao, B. Huang and Y. Li, *Angew. Chem., Int. Ed.*, 2020, **59**, 13021–13027.
16 K. Ma, J. Wu, X. Wang, Y. Sun, Z. Xiong, F. Dai, H. Bai, Y. Xie, Z. Kang and Y. Zhang, *Angew. Chem., Int. Ed.*, 2022, **61**, e202211094.
17 X. Zheng, Y. Xue, C. Zhang and Y. Li, *CCS Chem.*, 2022, 1–10.
18 D. Zhang, Y. Xue, X. Zheng, C. Zhang and Y. Li, *Natl. Sci. Rev.*, 2023, **10**, nwac209.
19 C. Xing, Y. Xue, B. Huang, H. Yu, L. Hui, Y. Fang, Y. Liu, Y. Zhao, Z. Li and Y. Li, *Angew. Chem., Int. Ed.*, 2019, **58**, 13897–13903.
20 W. Rong, H. Zou, W. Zang, S. Xi, S. Wei, B. Long, J. Hu, Y. Ji and L. Duan, *Angew. Chem., Int. Ed.*, 2021, **60**, 466–472.
21 H. Yu, Y. Xue, L. Hui, C. Zhang, Y. Fang, Y. Liu, X. Chen, D. Zhang, B. Huang and Y. Li, *Natl. Sci. Rev.*, 2021, **8**, nwaa213.
22 G. Shi, Y. Xie, L. Du, X. Fu, X. Chen, W. Xie, T. B. Lu, M. Yuan and M. Wang, *Angew. Chem., Int. Ed.*, 2022, **61**, e202203569.
23 X. Chen, X. Zheng, L. Qi, Y. Xue and Y. Li, *ACS Mater. Au*, 2022, **2**, 321–329.
24 Y. Gao, Y. Xue, F. He and Y. Li, *Proc. Natl. Acad. Sci. U. S. A.*, 2022, **119**, e2206946119.
25 Y. Gao, Y. Xue, L. Qi, C. Xing, X. Zheng, F. He and Y. Li, *Nat. Commun.*, 2022, **13**, 5227.
26 Y. Liu, Y. Gao, F. He, Y. Xue and Y. Li, *CCS Chem.*, 2022, 1–11.
27 X. Fu, X. Zhao, T. B. Lu, M. Yuan and M. Wang, *Angew. Chem., Int. Ed.*, 2023, e202219242.
28 H. Liu, H. Zou, D. Wang, C. Wang, F. Li, H. Dai, T. Song, M. Wang, Y. Ji and L. Duan, *Angew. Chem., Int. Ed.*, 2023, e202216739.
29 Y. Fang, Y. Xue, L. Hui, H. Yu and Y. Li, *Angew. Chem., Int. Ed.*, 2021, **60**, 3170–3174.
30 Y. Liu, Y. Xue, L. Hui, H. Yu, Y. Fang, F. He and Y. Li, *Nano Energy*, 2021, **89**, 106333.
31 M. Li, Q. Lv, W. Si, Z. Hou and C. Huang, *Angew. Chem., Int. Ed.*, 2022, **61**, e202208238.
32 N. Wang, J. He, K. Wang, Y. Zhao, T. Jiu, C. Huang and Y. Li, *Adv. Mater.*, 2019, **31**, e1803202.
33 W. Zhou, H. Shen, Y. Zeng, Y. Yi, Z. Zuo, Y. Li and Y. Li, *Angew. Chem., Int. Ed.*, 2020, **59**, 4908–4913.
34 Q. Yang, Y. Guo, B. Yan, C. Wang, Z. Liu, Z. Huang, Y. Wang, Y. Li, H. Li, L. Song, J. Fan and C. Zhi, *Adv. Mater.*, 2020, **32**, e2001755.
35 Q. Yang, L. Li, T. Hussain, D. Wang, L. Hui, Y. Guo, G. Liang, X. Li, Z. Chen, Z. Huang, Y. Li, Y. Xue, Z. Zuo, J. Qiu, Y. Li and C. Zhi, *Angew. Chem., Int. Ed.*, 2022, **61**, e202112304.
36 F. Wang, Z. Xiong, W. Jin, H. Liu and H. Liu, *Nano Today*, 2022, **44**, 101463.
37 F. Wang, Z. Zuo, L. Li, F. He, F. Lu and Y. Li, *Adv. Mater.*, 2019, **31**, e1806272.
38 J. Guo, M. Guo, F. Wang, W. Jin, C. Chen, H. Liu and Y. Li, *Angew. Chem., Int. Ed.*, 2020, **59**, 16712–16716.
39 X. Fu, F. He, J. Gao, X. Yan, Q. Chang, Z. Zhang, C. Huang and Y. Li, *J. Am. Chem. Soc.*, 2022, **145**, 2759–2764.
40 N. Chen, Y. n. Yang, F. He, Y. Li, Q. Liu and Y. Li, *Matter*, 2022, **5**, 2933–2945.
41 J. Hu, S. Li, J. Chu, S. Niu, J. Wang, Y. Du, Z. Li, X. Han and P. Xu, *ACS Catal.*, 2019, **9**, 10705–10711.
42 M. Yang, Y. X. Li, M. Jiang, P. H. Li, S. H. Chen, J. H. Liu, C. H. Lin, X. J. Huang and W. Q. Liu, *Small*, 2020, **16**, e1906830.
43 B. Zhang, L. Wang, Y. Zhang, Y. Ding and Y. Bi, *Angew. Chem., Int. Ed.*, 2018, **57**, 2248–2252.
44 Y. Huang, R. J. Nielsen, W. A. Goddard III and M. P. Soriaga, *J. Am. Chem. Soc.*, 2015, **137**, 6692–6698.
45 C. C. McCrory, S. Jung, J. C. Peters and T. F. Jaramillo, *J. Am. Chem. Soc.*, 2013, **135**, 16977–16987.

 